Thermodynamic properties of minerals and fluids

Alekhin Yu.V.[1], Fiaizullina R.V.[1,2] Basic valence mercury forms in gas-vapor mixtures, in thermal waters and in atmospheric air

[1] M.V. Lomonosov Moscow State University, Department of Geology, Moscow

[2] Institute of Geology of Ore Deposits, Petrography, Mineralogy and Geochemistry RAS, Moscow

alekhin@geol.msu.ru ; rinutiya@mail.ru

Abstract. The report is devoted to the discussion of mercury transport in gas-hydrothermal (two-phase) fluid systems. The estimation of the integrated flux density of mercury in the zone of unloading of the Kamchatka term is given by the example of two objects: the caldera of volcano Uzon and the Apapel Springs. On the basis of detailed studies of the $Hg^0_{(g)}-H_2O$ system, it was shown that at low temperatures and the standard volatility of oxygen in the atmosphere (in natural settings), not Hg^0 pairs but mercury oxide (HgO) dominate. In the liquid phase, mercury concentrations are ensured by the solubility of montroidite, determined by the hydroxyl complex such as $Hg(OH)_2$. A study of the solubility of mercury oxide under the univariant equilibrium of $Hg_{(g)}-HgO_{(s)}-H_2O$ under oxidizing and reducing conditions has shown that in most natural environments (Kamchatka's terms, atmosphere) at low temperatures, the forms of Hg(II) dominate and only in reducing conditions and temperatures of more than 100–120°C, Hg^0 predominates in the gas and liquid phases.

Keywords: mercury, mercury forms, Henry's coefficients, mercury solubility, HgO solubility.

Our element is interesting for its ability not only to be in two phases of thermal springs at once in three valence states, sometimes in comparable quantities, but also to be adsorbed in a definite manner at the gas-liquid interface. Evidence of this is also the washing out of mercury with rain under ordinary atmospheric conditions. In recent years, the situation in analytical geochemistry of mercury has significantly changed both in terms of reliable determination of low concentrations (Laperdina, 2000; Laperdina, 2005; Alekhin et al., 2010) and in the part of the possibilities of mobile phase analysis directly at the site of sampling (Mukhamadiyarova, 2011). New possibilities arose in the interpretation of the data obtained earlier with respect to the forms of transport and flux densities. Comparative analysis in this work we build only in terms of its own and Lary data for two objects: the caldera of volcano Uzon and the Apapel Springs. This is enough to extend the conclusions and results to other terms that broaden the concept of geochemical features of behavior and patterns of migration of mercury forms in the conditions of the Kamchatka term, including aerosol transport with a droplet liquid phase.

Review of studies of ore formation processes in the caldera Uzon can be found in (Bychkov, 2009). The necessary data on the geological structure, hydrothermal activity and the structural position of the caldera are also given there. Despite frequent statements by researchers that the ore formation in the caldera is also mercury, it seemed to us necessary to recheck this statement by balance calculations of mercury flux density and estimates of the fraction of its elementary form. According to preliminary estimates, Yu.V. Alekhin, G.A. Karpov et al. (Alekhin et al., 1987) the total reserves of the mercury of the Uzon were determined as 200 tons, based on data on its contents in the sediments of the Eastern thermal field. However, the reliability of the determination of mercury in the 1980s-1990s was clearly inadequate. For the last 15–20 years, the metrological assurance of the analyzes, in terms of the limits of detection and the analytical correctness of the results, has significantly increased. We present several estimates made by us, based on our recent analytical data (Fiaizullina, Alekhin, 2015). In this paper, the tables give the results of determinations of mercury content in geyserites, paleogeiserites, thermal and mud boilers, and also in soils. A high level of mercury content is associated mainly with the accumulation of it in clay minerals at the temperature barrier.

The total area of the Eastern thermal field (I, II and III sites) is close to 0.3 km^2. Then the volume of the plate 1 m thick, to which the sulphide ore occurrence is timed, is $3 \cdot 10^5$ m^3 and its mass is close to $5 \cdot 10^5$ tons. From the data processing (Fiaizullina, Alekhin, 2015) on variations in mercury content, it follows that the averages are close to 2.34 and 2.26 g/t, respectively, and an estimate of the amount of mercury in a 1 m thick plate results in mercury reserves of 1.15 tons, and this estimate is somewhat overestimated. Let us approach this problem on the other hand by estimating the flux density of mercury coming from the bowels of the caldera. We, like our predecessors (Bychkov, 2009; Alekhin et al., 1987; Ozerova, 1986; Sorokin et al., 1988; Ozerova et al., 1988), had no doubts that in the depths of the geothermal system, elemental mercury as a form of transport dominates, and in general for the caldera, the removal of mercury is very significant (Ozerova, 1986).

The central problem is the balance of removal and arrival of mercury with gas and liquid phases. Let us estimate (Mukhamadiyarova, 2011) the integral flux density of mercury in the unloading zone term. Let's consider three independent variants of calculation as extreme cases: 1. With a known area of the ore field (II section of the Eastern thermal field), 0.5×0.25 km ($1.25 \cdot 10^5$ m^2) and the known water flow rate of this section is 23.4 L/sec, we

calculate the flux density with an average mercury concentration of 1.5 μg/L ([1.5 μg/L×23.4 L/sec]/[1.25×10^5 m^2]=10·ng·m^{-2}·h^{-1}). If we arbitrarily extend this very significant estimate of the flux density to the area of the entire caldera of 15 km^2, we obtain a mercury production rate of only 1.3 kg/year. 2. Using the same value of the average gross mercury concentration of 1.5 μg/L, we follow, following Averyev V.V. (Averyev, 1966), which for all thermoregulations of the Uzon caldera assumed a thermal flow rate equal to 80 L/sec. For the same area of 15 km^2, we obtain a flux density of 28.8 ng·m^{-2}·h^{-1}. In this case, the estimation of the integrated production rate of mercury will be 3.8 kg/year. 3. If its main quantity does not dissipate with steam, but accumulates in the thickness of hydrothermalites and thermal waters, we use the concentration of mercury in the lake. Chloride, as the maximum of known to us on the Uzon (10.8 mkg/L). In this case, with a known total runoff of the lake's thermal waters 12 L/ sec, from an area of 150×200 m, provided the system is stationary, i.e. constancy of the composition with equal parity and consumption of thermal waters with a concentration of 10.8 μg/L, we obtain the value of the integrated production rate of mercury in the lake Chloridnoe 4.1 kg/year. Even if from this condition of stationarity, but also the accumulation of mercury in the depths of the geothermal system, we recalculate the entire caldera area of 15 km^2, we obtain a value of 205 kg/year. Let us compare these calculations with the mercury discharge in the source of the river Shumnaya. According to our data, the concentration of mercury in the water of the source of the river is 0.5 μg/L (KMCH-09/48 sample ((Fiaizullina, Alekhin, 2015), Table 3) with variations in the production rate of 4.8−9.6 m^3/sec by the number of meteorological precipitations. Direct measurements of flow rate (A. Yu. Bychkov, personal communication) in the summer of 1987 yielded 6.7 m^3/sec, which is close to an average estimate of 7.2 m^3/sec according to meteorological observations in 2009. If the flow rate is assumed to be 7.0 m^3/sec, we get the mercury discharge from the caldera, equal to 110 kg/year. Using this value, we can calculate the maximum flux density of the deep mercury emission taking into account the total area of thermal fields, estimated as 1.1 km^2. This leads us to a flux density of 100 kg·km^{-2}·year^{-1} or an average of 11400 ng·m^{-2}·h^{-1}. Of course, this estimate is not so much as maximum, as formal, for a number of reasons. We do not have any data that would indicate that at the present time there is no further extraction of mercury previously accumulated and dispersed in the thickness of the caldera deposits. Therefore, such an estimate may be overstated, but it is quite realistic. Another important thing is that extrapolating these data to the parameters of the deep fluid (250°C, $p(H_2O)$=40 bar) using the value of the Henry's constant leads to the value of the mole fraction of mercury vapor $X_{Hg(0)}$=0.0025 at a partial pressure Hg^0 equal to 10^{-1} bar, which seems absolutely unrealistic. Thus, an estimate of 11.400 ng·m^{-2}·h^{-1} hardly refers to elemental mercury as the main form of transport. If we consider this estimate to be realistic, we are forced to assume that the deep transport of mercury with the gas-vapor phase occurs in the form of other forms with high vapor pressure, for example, hydrate and chloride complexes.

Undoubted are the following facts: 1) the concentration of mercury in filtered water of river Shumnaya 0.5 μg/L is an extraordinary quantity and has never been observed in the fresh waters of the continent. The source of mercury can only be hydrothermalites and thermal waters; 2) in the atmospheric air above the Uzon thermal platforms, we do not observe high concentrations of elemental mercury capable of emission, and from this we conclude that oxidized forms of mercury predominate in the system in the unloading zone; 3) measurements of the flux density in the unloading zone do not give direct information about the scale and forms of mercury entering with the deep fluid; 4) the excess of mercury concentration in the atmospheric air of thermal fields over the local background (3.2−3.9 ng/m^3) and in the unloading area, with a total geometric mean of 7.1 ng/m^3, shows that the intake of endogenous Hg^0 The atmosphere from the surface of thermal fields is relatively small. According to our estimates, the mercury discharge with gas vapor phase in the II section of the Eastern thermal field corresponds to a value of 3.9 ng·m^3×2.17 m^3/sec=8.46 ng/sec or for the area of this section corresponds to an average mercury flux density of 0.24 ng·m^{-2}·h^{-1}. We are again convinced by comparing the two flux densities for section II (10 and 0.24 ng·m^{-2}·h^{-1}) that the main mercury transport in the upper part of the section, i.e. In the area of system unloading, occurs not with the gas phase and not in the form of Hg^0. An estimate of 10 ng·m^{-2}·h^{-1} is carried out through oxidized forms of mercury in the aqueous phase. Conventional concentrations of the order of 1.5 μg/L according to our data on Henry's constant values (Fiaizullina, Alekhin, 2015; Averyev, 1966) can in no way be determined by the dissolved form of Hg^0 in the unloading zone. Let us demonstrate this statement by a simple calculation. At 50−100°C in the unloading zone, the Henry's constant (Alekhin et al., 2011) lg K_H=-2.43 and K_H=0.0037=$m_{Hg(0)}/p_{Hg(0)}$ are practically constant. If we assume that the elementary form in the waters in the unloading area is elemental mercury (1.5 μg/L), then we arrive at the value $p_{Hg(0)}$=2.02·10^{-6} atm, which corresponds to the average volume concentration in the surface Air of about 17 000 ng/m^3! In the Uzon caldera, at any of the observation points, the measured values in the surface air did not

exceed 12−15 ng/m^3. Using the value of 10 ng·m^{-2}·h^{-1} for the flux density of oxidized forms of mercury, and assuming that all of the mercury in the interior of the stationary system is initially represented by the Hg^0 form in the gas-vapor phase, we can assume that the density of the deep emission flux at the Uzon is close to this value. Recall that the flux densities measured by us in zones of tectonic activity in other regions fall within a relatively narrow interval of 1.1−2.1 ng·m^{-2}·h^{-1}. In this respect, the density of the reconstructed deep flow of mercury for the ore field (10 ng·m^{-2}·h^{-1}) caldera of volcano Uzon is a very significant quantity. However, the main amount of mercury in the transport stage is oxidized and the flux density of atomic mercury on the surface does not exceed 0.24 ng·m^{-2}·h^{-1}, and resemble the standard situation of platform situations.

Apapel thermal springs are an example of Kamchatka, which is rare for cinnabar mineralization. More detailed analytical information on the composition of the water is given in our earlier works, for example in (Alekhin et al., 2009), and here we give only key information for solving the issue of valence forms and distribution of mercury between fluid phases. According to our literature data (Sorokin et al., 1988), an important difference between the thermal waters of the Apapel Springs from the waters of the Uzon caldera is the very low concentrations of dissolved hydrogen sulfide of the order (1.5−7)·10^{-7} m at the usual values for the caldera of volcano Uzon up to 10^{-4}−10^{-3} (by the molarity of H_2S). This contradiction, undoubtedly, is solvable only in the version of domination and in the waters of the Uzon in the zone of unloading of oxidized and complex forms of mercury. The high values of mercury content in the condensates of the Apapel thermal springs (24-1180 μg/L) and the recalculation of the volumetric concentration of mercury in the air by the mass of the condensate, allow us to establish that the data on mercury distribution between the gas and liquid phases are in clear contradiction with ours (Alekhin et al., 2011) refined data on the Henry's Hg^0 constants and mercury concentrations in the aqueous phase of the terms (log $K_{H(298)}$=−2.41; log $K_{H(373)}$=−2.43). Earlier they could be explained only in the version of the significant concentration of mercury Hg^0 on the surface of droplets of aqueous aerosol phases with additional extraction of mercury from the gas phase. An alternative version is the variant of the presence in the gas phase of other volatile Hg complexes.

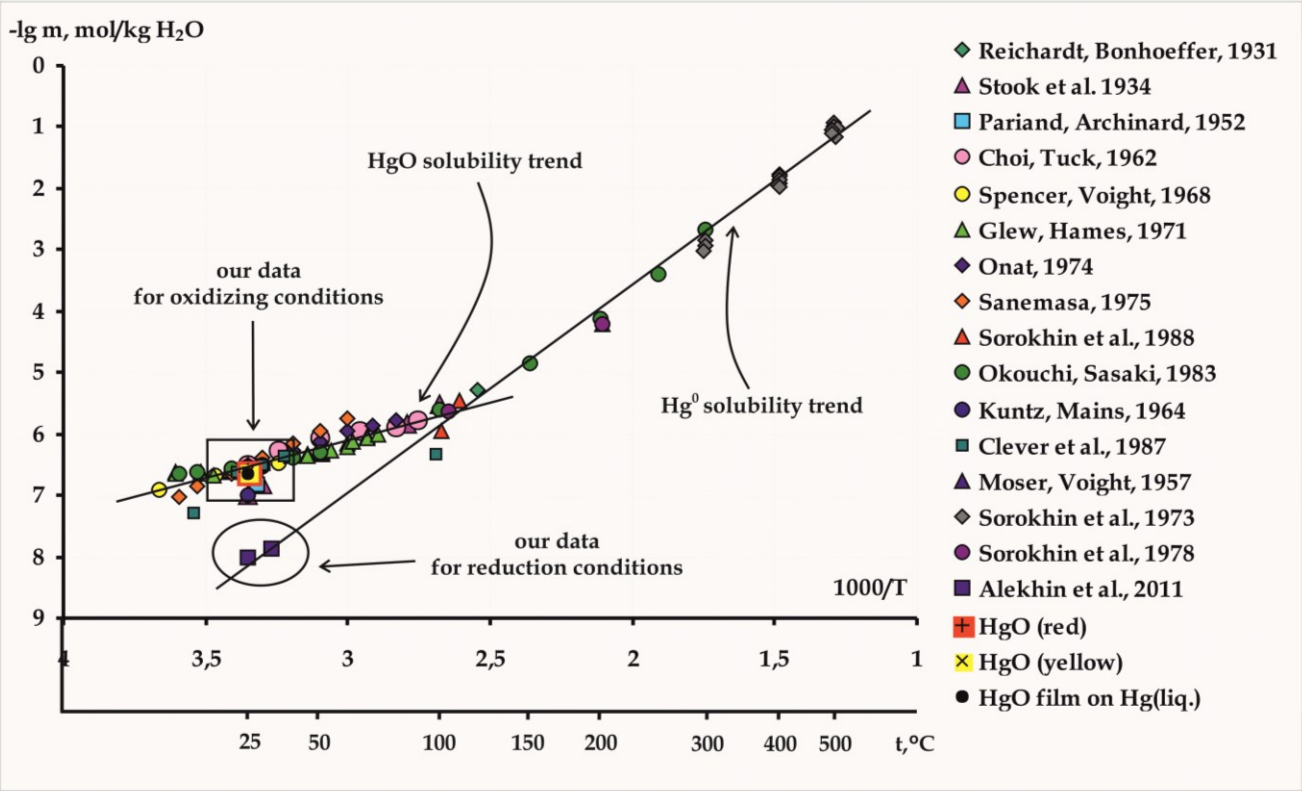

Fig. 1. Data on the joint solubility of $Hg^0_{aq.}$ and HgO at different temperatures

Using the enthalpy and heat capacity data for $HgO_{(g)}$ (Chase, 1951), we performed thermodynamic calculations for the reaction: $HgO_{(g)}=Hg^0_{(g)}+½O_{2(g)}$. Our task was to show, by using the data on the constant of this homogeneous equilibrium, what conclusions can be reached about the equilibrium of the valence forms in the gas phase and the distribution of the dominant forms of mercury in the

liquid and gas phases of two-phase fluids, using data on the elasticity of intrinsic vapors over Hg^0 and HgO. The problem was that it is usually assumed that there is no HgO vapor in the thermal dissociation of montroidite − $HgO_{(s)}$. However, such an interpretation of the experimental data in experiments on the thermal disassociation of this solid phase in vacuum (Taylor, 1962; Kazenas, Tsvetkov, 2008; Gorbacheva et al., 1998; L'vov, 1999) is not the case that we need to consider as a function of the vapor pressure (volatility) of oxygen in natural systems. For a simple equilibrium of these gas forms, we confined ourselves to considering the temperatures 0; 25 and 100°C. At 0°C lg K_{273}=−1.935, at 25°C lg K_{298}=−1.623 and at 100°C, log K_{373}=−0.937. For the temperature range 0−25°C we use the average volatility of oxygen in the atmospheric air ($f(O_2)$=0.204, log $f(O_2)$=−0.69). Hence, it is easy to calculate the ratio of volatilities and the proportions of Hg^0 and HgO vapor for a given oxygen fugacity: lg $f_{Hg(0)}$−lg f_{HgO}=log K−½ log $f(O_2)$. For 0°C, lg $f_{Hg(0)}$−lg f_{HgO}=−1.59 and a molar ratio of Hg^0/HgO=0.026 (i.e., the fraction of Hg^0 vapor is only 2.6%). For 25°C, a similar calculation leads us to the molar ratio Hg^0/HgO=0.053. Somewhat more complicated, but more convex this ratio changes at 100°C. The point is that in this case we must already take into account the increasing contribution of water vapor pressure to the sum of the partial pressures in the gas phase. Let $f(H_2O)$=0.5, while maintaining the proportions between the remaining gases of the atmosphere. Then the contribution of 20% O_2 at p=1 will correspond to $f(O_2)$=0.1, so that at lg K=−0.937·(lg $f_{Hg(0)}$−lg f_{HgO})=log K−½lg $f(O_2)$ =−0.887. Under these conditions, the ratio of mole amounts corresponds to 13% Hg^0 in the gas phase. At higher temperatures and lower volatilities of oxygen (lg $f(O_2)$=−2÷−3), according to calculations in the gas phase, the pairs Hg^0 begin to dominate. It is also important to determine the Henry's constant of gaseous HgO. We obtained from the proper and published data on the interpretation of the solubility of HgO the value lg K_{298}=lg m-log f(HgO)=−2.61.

The solubility of montroidite in water (HgO (s)) is sufficiently high (51.28 μg/kg H_2O or 2.37 10^{-7} mol/kg at 298.15 K) and is substantially higher than the solubility of elemental mercury in water (1.95 Mg/kg H_2O or 9.72 10^{-9} mol/kg) under the same conditions (Alekhin et al., 2011_1; Alekhin et al., 2011_2). These nontrivial results were obtained by us in interpreting our own and numerous experimental data (Sorokin et., 1988; Alekhin et al., 2011_1; Alekhin et al., 2011_2; Sorokin, 1973; Sorokin et., 1978) by the so-called "solubility of liquid mercury in water". Without resorting to detailed thermodynamic calculations, it is sufficient to plot data on the equilibrium solubility of montrodite (Remi, 1974) to understand that with the volatility of oxygen in the atmosphere we have a univariant equilibrium of the aqueous solution with liquid mercury and the oxide HgO film on its surface (fig. 1).

This concentration ratio and the fugacities of two forms, including for sufficiently labile in water or in a two-phase gas-vapor equilibrium mixture $Hg^0_{(g)}+HgO_{(g)}+H_2O=Hg_2^{2+}+2OH^-$ determines not only the ratio Hg^0 concentration and HgO in the aqueous phase (lg $m_{Hg(0)}$=−8.01 and lg m_{HgO}=−6,63), but also as a result of the heterophase redox disproportionation process (Alekhin et al., 1992) provides the elution of the oxidized form of the gas phase with the appearance of liquid water, which removes a number of previously unexplained contradictions numerous observations of the dynamics of changes in mercury concentrations in those max Kamchatka, and in the air. Practically all the experimental data for two univariant equilibria are collected in this figure (fig. 1): water (L_2) − liquid mercury (L_1) − monthroidite (S) and water-liquid mercury-gas (G, mixture of water vapor, atomic mercury and HgO). Their intersection at 108.2±3°C determines the temperature of the nonvariant point L_1L_2SG.

References:

1. Alekhin Yu.V., Dadze T.P., Zotov A.V., Karpov G.A., Mironova G.D., Sorokin V.I. Conditions for the formation of the modern sulfide mercury-antimony-arsenic mineralization of the Uzon caldera (Kamchatka) // Volcanology and seismology, 1987. N2. P. 34−43. In Russ.
2. Alekhin Yu.V., Pokrovsky O.S., Vakulenko A.G. Potentiometric study of thermodynamic properties of mercury ions Hg_2^{2+} and Hg^{2+} at 25−150°C in nonisothermal cell with transference // Experiment in Geosciences. 1992. Vol. 4. N 4. P. 21−22.
3. Alekhin Yu.V., Karpov G.A., Lapitsky S.A., Mukhamadiyarova R.V., Nikolaeva A.G. Behavior of mercury in the Apapel thermal springs (Kamchatka) // Volcanism and geodynamics: Proceedings of the IV All-Russian Symposium on Volcanology and Paleovolcanology. Vol.2. Petropavlovsk-Kamchatsky: IVS FEB RAS. 2009. P. 688−690. In Russ.
4. Alekhin Yu.V., Mukhamadiyarova R.V., Smirnova A.S. Methodological research in the field of geochemistry of low mercury content in conjugated geochemical reservoirs // Materials of the International Symposium "Mercury in the Biosphere: Ecological and Geochemical Aspects". Moscow: Vernadsky Institute RAS. 2010. P. 43−47. In Russ.
5. Alekhin Y.V., Zagrtdenov N.R., Mukhamadiyarova R.V. Hg^0(liq)–Hg^0(solution) equilibrium and solubility of elementary mercury in water // Moscow University Geology Bulletin, 2011. Vol. 66. N. 6. P. 439–441.
6. Alekhin Yu.V., Zagrtdenov N.R., Mukhamadiyarova R.V. Experimental research of metal mercury solubility in water // Goldschmidt Conference Abstracts. 2011. P. 421.

7. Averyev V.V. Hydrothermal process in volcanic areas and its connection with magmatic activity // Modern volcanism. Proceedings of the Second All-Union Volcanological Conference September 3-17. Moscow: Nauka, 1966. Vol. 1. P. 118–128. In Russ.
8. Bychkov A.Yu. Geochemical model of modern ore formation in the Uzon caldera (Kamchatka). Moscow: GEOS, 2009. − 124 p. In Russ.
9. Chase M.W. Jr. NIST-JANAF Thermochemical tables, fourth edition // J. Phys. Chem. Ref. Data, 1998. Monograph 9. P. 1−1951.
10. Gorbacheva M.V., Mayorova A.F., Mudretsova S.N., Rudniy E.B., Rusin A.D. Thermodynamic properties of mercury oxide // J. Phys. Chem. in Russ, 1998. Vol. 72. N3. P. 416−420. In Russ.
11. Kazenas E.K., Tsvetkov Yu.V. Thermodynamics of oxides evaporation. Moscow:LKI, 2008. − 480 p. In Russ.
12. Laperdina T.G. Determination of mercury in natural waters. Novosibirsk: Nauka, 2000. − 222 p. In Russ.
13. Laperdina T.G. Determination of the forms of mercury in environmental objects // Mercury. Problems of geochemistry, ecology, analytics. Collection of scientific papers. Moscow: IMGRE, 2005. P. 62−97. In Russ.
14. L'vov B.V. Kinetics and mechanism of thermal decomposition of mercuric oxide // Thermochimica Acta, 1999. N 333. P. 21−26.
15. Mukhamadiyarova R.V. Investigation of emission fluxes, evasion and mechanisms of inter-reservoir migration of mercury // Bulletin of the Moscow Society of Nature Testers. Geological Department. Moscow: MSU, 2011. Vol. 86. Issue 6. P. 64−71. In Russ.
16. Ozerova N.A. Mercury and endogenic ore formation. Moscow: Nauka, 1986. – 230 p. In Russ.
17. Ozerova N.A., Shikina N.D., Borisov M.V. et al. Mercury in the modern hydrothermal process // Modern hydrothermal and mineral formation. Moscow: Nauka, 1988. P. 34–49. In Russ.
18. Remi G. Course of Inorganic Chemistry. Vol. II. Moscow: Mir, 1974. − 776 p. In Russ.
19. Sorokin V.I. The solubility of mercury in water in the temperature range 300−500°C and pressures of 500−1000 atm // Reports of the Academy of Sciences of the USSR, 1973. Vol. 213. N4. P. 852−855. In Russ.
20. Sorokin V.I., Alekhin Yu.V., Dadze T.P. The solubility of mercury in Hg−H_2O, HgS−(Cl)−H_2O systems and the forms of its existence in the sulfide-forming thermal waters of Kamchatka and Kunashir Islands // Essays on physico-chemical petrology. Moscow: Nauka, 1978. Issue 8. P. 133−149. In Russ.
21. Sorokin V.I., Pokrovsky V.A., Dadze T.P. Physicochemical conditions of formation of antimony-mercury mineralization. Moscow: Nauka, 1988. – 144 p. In Russ.
22. Taylor D. Thermal decomposition of mercury oxide // J. Chem. Soc., 1962. Jan. PP. 1047−1050.
23. Fiaizullina R.V., Alekhin Yu.V. Mercury in atmospheric air, gas vapor condensates and waters of the term Kamchatka // Materials of the II International Symposium "Mercury in the Biosphere: Ecological and Geochemical Aspects". Novosibirsk: IIC SB RAS, 2015. P. 380−384. In Russ.

Eremin O.V.[1], Filenko R.A.[1], Epova E.S.[1], Rusal' O.S.[1], Buchinskii V.A.[2]. Evaluation of standard Gibbs energies of the minerals alunite group from the supergene zone of tin-polymetallic deposit Sherlovaya Gora (Transbaikalia).

[1] Institute of natural resources, ecology and cryology of SB RAS, Chita,
[2] A.P. Vinogradov Institute of Geochemistry SB RAS, Irkutsk (yeroleg@yandex.ru)

Abstract. The standard Gibbs energy of formation from the elements for minerals of complex compositions of the alunite group – philipsbornites, segnitites, beudantites, beaverites, and jarosites from the rock dumps of the tin-polymetallic deposit Sherlovaya Gora (Transbaikalia) were calculated on the basis of constituent oxides and crystal water additivity. The obtained characteristics for 41 minerals were included in the PC database "Selector" and can be used in the geochemical calculations with their participation.

Keywords: Sherlovaya Gora, alunite group minerals, constituent oxides, standard Gibbs energy.

More than a hundred of supergene minerals were discovered and identified in the area of oxidization zone of the tin-polymetallic Sherlovaya Gora deposit (Transbaikalia) [Kasatkin et al., 2014]. Widespread in components of the mining landscape is typical for toxic elements such as arsenic and lead. Minerals of lead hydroxoarsenates(sulphates) represent the natural accumulators of these toxic elements (Pb and As) due to their poor solubility in aqueous solutions [Frost et al., 2011]. To assess the conditions of formation and stability of minerals in this class it is necessary to know the values of their thermodynamic characteristics, particularly for isobaric-isothermal conditions – the values of standard Gibbs energies. This paper presents the evaluation of standard Gibbs energies of formation from the elements of 41 minerals of the alunite group, selected on the tailings of tin deposit and career for which the chemical compositions (formulas) have been determined [Kasatkin et al., 2014]. Figure 1 presents some minerals of alunite group from Sherlovogorskoe deposit.

Fig. 1. Minerals segnitite (left**) and jarosite (**rigth**) from quarry dumps of Sherlovogorskoe deposit (Photo by R. A. Filenko).**

Table 1. The values of the standard Gibbs energies of oxides used in the additive scheme (1) to calculate the potentials of minerals of the alunite group.

Oxides	-G, J/mole	References
K_2O	320700	[Yokokawa, 1988]
PbO	188950	-
Al_2O_3	1582280	-
CuO	129500	-
ZnO	318320	-
Fe_2O_3	742099	-
As_2O_5	782400	-
SiO_2	856322	-
P_2O_5	1371700	[Quick reference, 1983]
SO_3	371170	-
H_2O	250000	[Eremin et al., 2016; Eremin, 2015]

Table 2. The values of the standard Gibbs energies of formation from the elements of alunite group minerals, calculated by the additive scheme (1). The numbering of the minerals (the left column) refers to data from [Kasatkin et al., 2014].

№	Minerals formulas	-G, J/mole
	Philipsbornites	
1	$Pb_{0.97}Al_{2.89}Fe_{0.16}As_2O_{7.09}(OH)_{6.91}$	2117438
2	$Pb_{0.99}Al_{2.8}Fe_{0.23}As_2O_{7.07}(OH)_{6.93}$	2142571
3	$Pb_{1.03}Al_{2.69}Fe_{0.35}As_2O_{7.18}(OH)_{6.82}$	2172202
4	$Pb_{0.96}Cu_{0.32}Al_{2.68}Fe_{0.04}As_{1.81}Si_{0.13}S_{0.06}O_{6.65}(OH)_{7.35}$	2210113
5	$Pb_{1.04}Cu_{0.44}Al_{2.61}As_2O_{6.79}(OH)_{7.21}$	2143625
6	$Pb_{1.05}Cu_{0.23}Zn_{0.18}Al_{2.32}Fe_{0.27}As_{1.64}Si_{0.36}O_{6.33}(OH)_{7.67}$	2477801
7	$Pb_{1.04}Cu_{0.73}Al_{2.24}As_2O_{6.26}(OH)_{7.74}$	2218158
8	$Pb_{0.94}Al_{2.04}Fe_{1.03}As_2O_{7.09}(OH)_{6.91}$	2367336
9	$Pb_{0.99}Al_{2.02}Fe_{0.97}As_2O_{6.95}(OH)_{7.05}$	2370438
10	$Pb_{1.04}Al_{1.88}Fe_{1.07}As_2O_{6.93}(OH)_{7.07}$	2408415
11	$Pb_{1.01}Al_{1.80}Fe_{1.16}As_2O_{6.90}(OH)_{7.10}$	2433562
12	$Pb_{0.95}Cu_{0.37}Al_{1.73}Fe_{0.94}As_{1.77}Si_{0.03}S_{0.2}O_{6.82}(OH)_{7.18}$	2402918
13	$Pb_{1.03}Al_{1.68}Fe_{1.27}As_2O_{6.91}(OH)_{7.09}$	2467412

№	Minerals formulas	-G, J/mole
	Segnitites	
14	$Pb_{1.02}Al_{1.42}Fe_{1.53}As_2O_{6.89}(OH)_{7.11}$	2543926
15	$Pb_{0.93}Cu_{0.38}Zn_{0.21}Al_{0.67}Fe_{1.74}As_2O_{6.27}(OH)_{7.73}$	2739063
16	$Pb_{0.97}Al_{1.22}Fe_{1.82}As_{1.31}Si_{0.62}S_{0.07}O_{6.51}(OH)_{7.49}$	2960734
17	$Pb_{1.01}Al_{1.23}Fe_{1.82}As_{1.98}Si_{0.02}O_{7.15}(OH)_{6.85}$	2611412
18	$Pb_{1.00}Al_{1.20}Fe_{1.83}As_2O_{7.09}(OH)_{6.91}$	2609057
19	$Pb_{1.05}Cu_{0.44}Al_{0.64}Fe_{1.89}As_{1.76}S_{0.24}O_{6.81}(OH)_{7.19}$	2683636
20	$PbCu_{0.69}Al_{0.27}Fe_{1.95}As_{1.77}Si_{0.01}S_{0.22}O_{6.25}(OH)_{7.75}$	2774606
21	$Pb_{1.05}Cu_{0.52}Al_{0.46}Fe_{2.05}As_{1.83}S_{0.17}O_{6.84}(OH)_{7.16}$	2736776
22	$Pb_{1.03}Cu_{0.4}Al_{0.44}Fe_{2.13}As_{1.76}S_{0.24}O_{6.81}(OH)_{7.19}$	2747906
23	$Pb_{1.06}Cu_{0.35}Zn_{0.24}Al_{0.3}Fe_{2.15}As_{1.4}Si_{0.29}S_{0.31}O_{6.67}(OH)_{7.33}$	2970825
24	$Pb_{1.04}Cu_{0.4}Zn_{0.28}Al_{0.2}Fe_{2.22}As_{1.5}Si_{0.3}S_{0.2}O_{6.6}(OH)_{7.4}$	3019920
25	$Pb_{1.02}Al_{0.41}Fe_{2.6}As_{1.56}P_{0.06}S_{0.38}O_{7.45}(OH)_{6.55}$	3570479
26	$Pb_{1.02}Al_{0.27}Fe_{2.7}As_{1.78}P_{0.02}S_{0.2}O_{7.15}(OH)_{6.85}$	3664660
27	$Pb_{1.05}Fe_{2.99}As_{1.61}Si_{0.18}S_{0.21}O_{7.1}(OH)_{6.9}$	3032251
	Beudantites	
28	$Pb_{0.97}Al_{0.6}Fe_{2.37}As_{1.35}P_{0.08}S_{0.57}O_{7.42}(OH)_{6.58}$	3422494
29	$PbCu_{0.41}Fe_{2.57}As_{1.35}S_{0.65}O_{7.15}(OH)_{6.85}$	2821272
30	$Pb_{1.04}Fe_3As_{0.51}S_{1.49}O_{8.57}(OH)_{5.43}$	2740961
31	$Pb_{1.05}Cu_{0.46}Zn_{0.33}Al_{0.21}Fe_{2.04}As_{0.56}P_{0.01}Si_{0.08}S_{1.35}O_{7.7}(OH)_{6.3}$	3347546
32	$Pb_{1.06}Cu_{0.47}Zn_{0.27}Al_{0.24}Fe_{2.03}As_{0.52}P_{0.04}Si_{0.09}S_{1.35}O_{7.67}(OH)_{6.33}$	3336353
33	$Pb_{1.05}Cu_{0.56}Zn_{0.14}Al_{0.28}Fe_2As_{0.61}S_{1.39}O_{7.73}(OH)_{6.27}$	2618041
	Beaverites	
34	$Pb_{1.05}Cu_{0.55}Zn_{0.23}Al_{0.25}Fe_{2.01}As_{0.47}Si_{0.1}S_{1.43}O_{7.77}(OH)_{6.23}$	2687443
35	$Pb_{1.03}Cu_{0.59}Zn_{0.23}Al_{0.3}Fe_{1.93}As_{0.44}P_{0.03}Si_{0.07}S_{1.46}O_{7.78}(OH)_{6.22}$	3246010
	PbFe-Sulphates	
36	$Pb_{1.03}Fe_{2.97}As_{0.36}S_{1.64}O_{8.61}(OH)_{5.39}$	2719936
37	$Pb_{1.01}Fe_{2.98}As_{0.3}S_{1.7}O_{8.66}(OH)_{5.34}$	2712416
	Pb- jarosite	
38	$K_{0.03}Pb_{0.46}Fe_{2.94}S_2O_{7.77}(OH)_{6.23}$	2703703
	Jarosites	
39	$K_{1.02}Fe_{2.96}S_2O_{7.9}(OH)_{6.1}$	2766703
40	$K_{0.66}Pb_{0.35}Cu_{0.31}Fe_{2.68}As_{0.26}S_{1.74}O_{7.76}(OH)_{6.24}$	2734068
41	$K_{0.94}Pb_{0.1}Cu_{0.01}Fe_3As_{0.28}S_{1.72}O_{7.88}(OH)_{6.12}$	2797015

The method of constituents oxides additivity was used for calculating the potentials of complex compositions minerals [Eremin, etc., 2015]:

$$G(mineral)=\sum k(i)G(oxide), \quad (1)$$

where k(i) are coefficients in the reactions of minerals formation from the oxides. The potential values of the oxides used in the calculations are given in table 1. The value of the free energy for crystal water $G(H_2Ocr)$=-250 kJ/mol was taken from the estimates of the potentials of minerals classes of arsenate and sulphoarsenates of iron, lead, zinc and copper [Eremin, 2015; Eremin, et al., 2016]. The numbering of the minerals formulas corresponds to the data of the work [Kasatkin et al., 2014]. For

example, the reaction of the beudantite (32) formation can be written:

$1.06PbO+0.47CuO+0.27ZnO+1.35SO_3+0.12Al_2O_3++ 1.015Fe_2O_3+0.26As_2O_5 + 0.02\ P_2O_5 + 0.09SiO_2 + 3.165H_2O$ = Beudanite (32).

Characteristics of the minerals (table 2) were included in the "Selector" databases and can be used in geochemical calculations.

References:

1. Eremin O. V., Rusal' O. S., Bychinskii V. A., Chudnenko K. V., Fomichev S. V., Krenev V. A. Calculation of standard thermodynamic potentials of sulfates and hydroxosulfates of aluminum//Russian Journal of inorganic chemistry. 2015. No. 8. P. 1048-1055. (In Russian)
2. Eremin O. V., Epova E. S., Bychinskii V. A. Equations for the calculation of standard Gibbs energies for minerals of iron sulphoarsenates/Materials of all-Russian conference with international participation "Biosphere Evolution and technogenesis", VI all-Russian Symposium with international participation "Mineralogy and Geochemistry of landscape of mountain-ore territories" and XIII all-Russian readings in memory of academician A. E. Fersman "environmental management", "Modern mineral formation", dedicated to the 35th anniversary of INREC SB RAS, 2016. P. 382-385. (In Russian)
3. Kasatkin A. V., Klopotov K. I., Plasil J. Supergene minerals of Sherlovaya Gora//Sherlovaya Gora. Mineralogical almanac. 2014. Vol. 19. vol. 2. P. 94-137. (In Russian)
4. Quick reference of the physico-chemical variables. Ed. 8 -. revised ed. by A. A. Ravdel and A. M. Ponomareva. L.: Chemistry, 1983. 232 p. (In Russian)
5. Eremin O. V. The Gibbs energy increments for minerals of Pb-jarosite group//Physical Chemistry: An Indian Journal. 2015, 10(3), p. 90-95.
6. Frost R. L., Palmer S. J., Spratt H. J., Martens W. N. The molecular structure of the mineral beudantite PbFe3(AsO4,SO4)2(OH)6 – Implications for arsenic accumulation and removal//Journal of Molecular Structure 988 (2011) 52-58.
7. Yokokawa H. Tables of thermodynamic properties of inorganic compounds//Journal of the national chemical laboratory for industry, 1988,Tsukuba Ibaraki 305, Japan, V. 83, 27-118.

Eremin O.V.[1], Mikhailov M.A.[2], Buchinskii V.A.[2]. Evaluation of Gibbs energies of formation from the elements for beryllium indialite.

[1]Institute of natural resources, ecology and cryology of SB RAS, Chita,

[2] A.P. Vinogradov Institute of Geochemistry SB RAS, Irkutsk (yeroleg@yandex.ru)

Abstract. On the basis of beryl and cordierite thermodynamics, the increments of the standard Gibbs energies of these minerals were calculated. The Gibbs energy value of beryllium indialite $Mg_2BeAl_2Si_6O_{18}$ was estimated by the additive scheme of oxide increments. The obtained data can be used for calculation of the free energies of the synthetic beryllium indialites in the Be-Mg-Al-Si-O system.

Keywords: beryllium indialite, the standard Gibbs energy.

Beryllium indialite (BI) $Mg_2BeAl_2Si_6O_{18}$ may present a promising material in the production of lasers, specific ceramics, cells of information in quantum computers, etc. In contrast to structural analogues of the minerals beryl ($Be_3Al_2Si_6O_{18}$) and cordierite ($Mg_2Al_4Si_5O_{18}$), beryllium indialite in nature to date, not discovered, however, simply can be obtained when cooled slightly superheated stoichiometric mixture of the constituent oxides (or salts) [Mikhailov and Demina, 2010]. This paper presents an algorithm for estimating the values of standard Gibbs energies of formation from the elements of BIs.

System Be-Al-Si-O

For the reaction of beryl formation from oxides:

$$3BeO + Al_2O_3 + 6SiO_2 = Be_3Al_2Si_6O_{18} \qquad (1)$$

the linear decompositions of the standard Gibbs energy of beryl G=-8500.5 kJ/mol [Robie and Hemingway, 1995] were obtained by the methods of linear programming [Eremin, 2014] for the constituents of the chemical elements (2) and oxides (3):

G(J/mole)=-8500500=-184707(Be) - 200915(Al)-55199(Si)-400741(O) (2)

G(J/mole)=-8500500= -583422(BeO) – 1590755(Al_2O_3) – 859913 (SiO_2) (3)

In the estimates of the Gibbs energies of the substances often used equation of constituent oxides additivity:

$$G=\sum \nu G(Oxides), \qquad (4)$$

where ν - the coefficients of the reactions of formation from oxides.

Equation (4) is characterized by high accuracy for anhydrous silicates. Based on equations (2-4) the calculations of Gibbs energies for compounds in the system Be-Al-Si-O and relative errors are presented in Table 1.

Table 1. Gibbs energy (J/mole), calculated according to the equations (2-4), δ –relative errors (%) - the second line in the table cell, <δ> is the average error for the used equation.

Minerals	-G, J/mole	(2)	(3)	(4)
Beryl $Be_3Al_2Si_6O_{18}$	8500500 [Robie and Hemingway, 1995]	8500500 0.00	8500500 0.00	8461118 0.46
Phenacite Be_2SiO_4	2028400 [Robie and Hemingway, 1995]	2027581 0.04	2026758 0.81	2016923 0.57
Chrysobery $BeAl_2O_4$	2178600 [Yokokawa, 1988]	2189505 0.50	2174177 0.20	2162580 0.74
Kyanite Al_2SiO_5	2443100 [Robie and Hemingway, 1995]	2460739 0.72	2450668 0.31	2438603 0.18
Mullite $Al_2Si_2O_{13}$	6441800 [Robie and Hemingway, 1995]	6525533 1.30	6492090 0.78	6459486 0.27
$BeO(Al_2O_3)_3$	5320416 [Yokokawa, 1988]	5397616 1.44	5355687 0.66	5327140 0.13
<δ>, %		0.67	0.46	0.39

System Mg-Al-Si-O

For the reaction of cordierite formation

$$2MgO + 2Al_2O_3 + 5SiO_2 = Mg_2Al_4Si_5O_{18} \quad (5)$$

decompositions of type (2-3) are

$$G=-8651100 = -141814(Mg)-140710(Al)+0.2(Si)-433644(O) \quad (6)$$

$$G=-8651100 = -590557(MgO) - 1582381(Al_2O_3) - 861039(SiO_2) \quad (7)$$

Calculations of the Gibbs energies according to equations (4,6,7) for compounds of Mg-Al-Si-O and error estimates are given in Table 2.

Table 2. Gibbs energy (J/mole), calculated according to the equations (4,6,7), δ – relative error (%), <δ> is the average error for the used equation

Minerals	-G, J/mole [Robie and Hemingway, 1995]	(6)	(7)	(4)
Cordierite $Mg_2Al_4Si_5O_{18}$	8651100	8651100 0.00	8651100 0.00	8585077 0.77
Forsterite Mg_2SiO_4	2053600	2018011 1.75	2042181 0.58	1995225 2.88
Pyrope $Mg_3Al_2Si_3O_{12}$	5934500	5910013 0.41	5937212 0.05	5859602 1.27
Enstatite $MgSiO_3$	1458300	1442554 1.09	1451610 0.46	1425774 2.26
Spinel $MgAl_2O_4$	2176600	2157808 0.87	2172952 0.17	2151731 1.15
Kyanite Al_2SiO_5	2443100	2449448 0.26	2443420 0.01	2438603 0.18
Mullite $Al_2Si_2O_{13}$	6441800	6481247 0.61	6469221 0.42	6459486 0.27
Sapphirine $Mg_2Al_4SiO_{10}$		5182714	5206943	5159785
<δ>, %		0.71	0.24	1.25

System Be-Mg-Al-Si-O

To estimate the Gibbs energy of BI by the reaction $2MgO + Al_2O_3 + 6SiO_2 + BeO = Mg_2BeAl_2Si_6O_{18}$, was used the decomposition (7) the oxide of increments plus a value for BeO from (3):

$$G= -590557*2 – 1582381*1 – 861039*6 – 583422*1 = -8513180 \text{ (J/mole)}.$$

The estimated error for the Gibbs energy of BI is around 0.5%. The used algorithm can be applied to assess the potential BI of arbitrary chemical compositions in the system Be-Mg-Al-Si-O. The potential values used in the calculations are given in Table 3.

Table 3. The values tof the standard Gibbs energies used in the calculations

Compounds	-G J/mole	
BeO	580300	[Yokokawa, 1988]
MgO	569451	[Robie and Hemingway, 1995]
Al_2O_3 (Corundum)	1582280	[Robie and Hemingway, 1995]
SiO_2 (Quartz)	856323	[Robie and Hemingway, 1995]
$Be_3Al_2Si_6O_{18}$(Beryl)	8500500	[Robie and Hemingway, 1995]
$Mg_2Al_4Si_5O_{18}$(Cordierite)	8651100	[Robie and Hemingway, 1995]

References:

1. Eremin O. V. Evaluation of standard thermodynamic potentials aluminosilicate of calcium, using methods of linear programming//Geokhimiya, 2014, No. 9, p. 859-864. (In Russian)
2. Mikhailov M. A., Demina T. V. Crystallization of beryllium indialite from its own melt in the oxidative conditions// crystallography, 2010, volume 55, no. 4, pp. 741-748. (In Russian)
3. Robie R. A. and Hemingway B. S. (1995), Thermodynamic properties of minerals and related substancies of 298.15 K and 1 bar pressure and at higher temperatures, U. S. Geol.Surv.Bull., 2113, Goverment Printing Office, Washington, 461 p.
4. Yokokawa H. Tables of thermodynamic properties of inorganic compounds//Journal of the national chemical laboratory for industry, 1988,Tsukuba Ibaraki 305, Japan, V. 83, 27-118.

Testov D.S.[1], Tyurin A.V.[2], Polotnyanko N.A.[1], Khoroshilov A.V.[2], Chareev D.A.[3], Gavrichev K.S.[2] Heat capacity and thermodynamic properties of crystalline platinum disulfide

[1]Dubna University, Dubna, [2]Institut of General and inorganic chemistry RAS, Moscow, [3]Institute of Experimental Mineralogy RAS, Chernogolovka Moscow district (polot.nat@gmail.com)

Abstract. From the noble metals platinum and its compounds are of particular interest to theoretical and physical chemical studies due to the unique properties and practical application in various fields, for example, in the instrument engineering and chemical industry. This work is devoted to study of the thermodynamic properties of the synthesized sample PtS_2(cr.) based on new calorimetric studies determined low – and high-temperature isobaric heat capacity.

Keyword: heat capacity, thermodynamic properties, platinum disulfide.

The thermodynamic properties of platinum disulphide were studied over a wide temperature range, as part of comprehensive studies of the thermodynamic properties of compounds logging to S-Pt phase diagram.

The sample PtS_2(cr.) was synthesized in a quartz ampoule from simple substances taken in a stoichiometric ratio at 1123.15 K with one intermediate mashing. The resulting black powder with a grain size of up to 0.1 mm was investigated by X-ray powder diffractometry on a diffractometer BRUKER (Cu$K_{\alpha1}$-radiation, Graphite monochromator). According to X-ray analysis, no phase impurities were detected. Also the absence of other phases was confirmed by electron probe microanalyzer.

The heat capacity of PtS_2 was measured with the by using an automated adiabatic vacuum calorimeter BKT-3 designed and manufactured at CJSC «Termis». The measurements were performed in automatic mode using a system: a computer, an analog control and data acquisition unit. The sample was loaded into a thin-walled titanium cylindrical container with an internal volume of 1 cm^3. The container was sealed in a special chamber in a helium atmosphere at a pressure of ≈ 0.3 bar. The temperature of calorimeter was measured by an iron-rhodium resistance thermometer. The design of the installation and the measurement procedure were described in detail in [Malyshev].

The sample mass was 0.41056 g. The molecular mass was calculated using atomic masses [http://www.physics.nist.gov/PhysRefData/Compositions] was 259.212 g/mol.

To calculate the standard thermodynamic functions in a wide temperature range the experimental data on the low-temperature heat capacity were analyzed and processed. This task was performed using spline approximation using to the program that was part of the mathematical software of the IVTANTHERMO data bank [Iorish]. The processing of the experimental data was carried out in two stages:

1) extrapolation of the heat capacity to 0 K;

2) smoothing of the experimental data taking into account the features of the dependence of Cp(T).

On the basis of measurement data of the isobaric heat capacity of PtS_2(cr.) in the temperature range of 5 – 345 K were obtained standard thermodynamic functions. At 298,15 K the following values were determined: $C_p°$ = 66,18±0,13 J/(mol·K), $S°$ = 74,51±0,15 J/(mol·K), $H°(298,15\ K)–H°(0)$ = 11,78±0,02 kJ/mol, $\Phi°$ = $-[G°(T)–H°(0)]/T$ = 35,00±0,07 J/(mol·K).

The results obtained using a synchronous thermal analyzer with a platinum furnace STA 449 F1 Jupiter® showed that in the range 345-875 K the sample PtS_2 was stable and had not got phase transformations (Fig. 2).

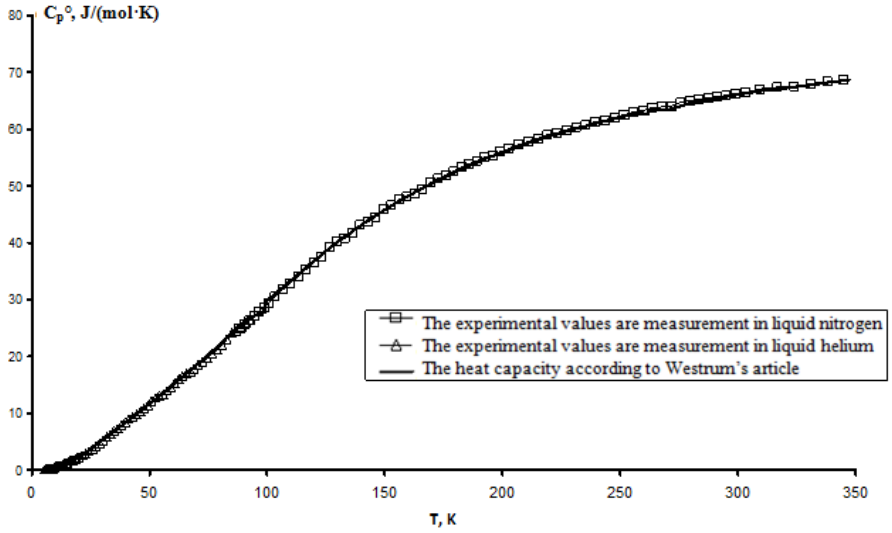

Fig. 1. Low-temperature heat capacity PtS_2

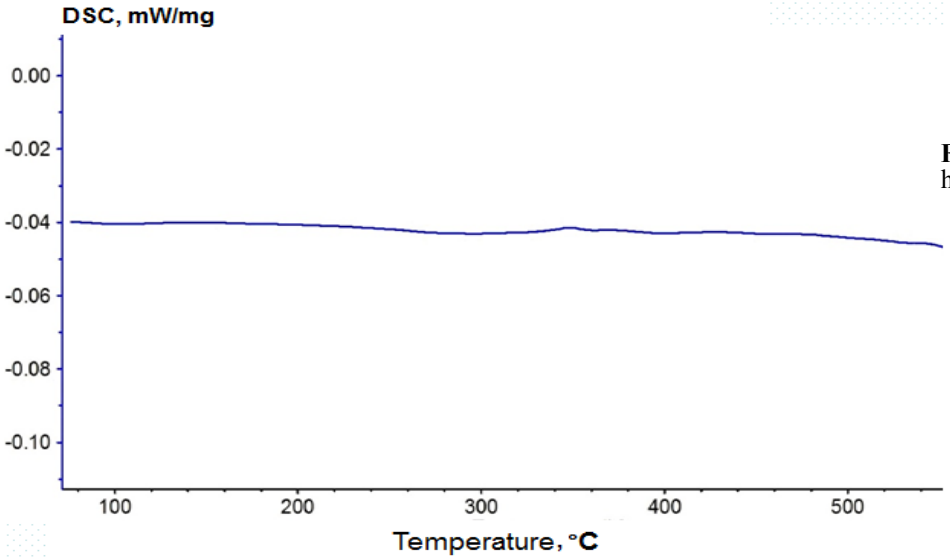

Fig. 2. Measurements of the heat flux of the sample PtS_2

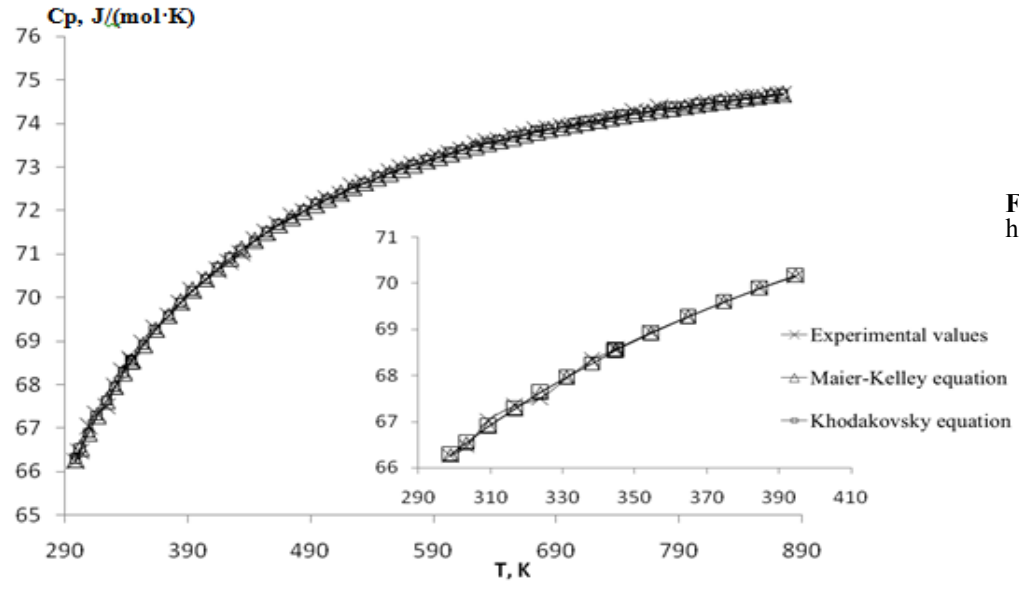

Fig. 3. High-temperature heat capacity PtS_2(cr.)

The results of a high-temperature measurement of the heat capacity by the method of differential scanning calorimetry at 54 points are shown in Fig. 3.

The results of experimental determination of the isobaric heat capacity of crystalline substances at temperatures above 298.15 K could be represented by approximation by empirical or semiempirical equations [Khodakovsky]. In present paper the Mayer-Kelly (1) and Khodakovsky (2) nonlinear regression equations parametres for the heat capacity of crystalline platinum disulphide (Fig. 3) were calculated and the adequacy of the models:

$$C_p^\circ = 74.98 + 8.53\cdot10^{-4}\cdot T - 8.00\cdot10^{5}\cdot T^{-2} \quad (1)$$

$$C_p^\circ = 78.92 - 3Rn\,(36.55\cdot T^{-1} + 39.20\cdot T^{-2} + 1.11\cdot10^{6}\cdot T^{-3}) - 1.16\cdot10^{-3}\cdot T \quad (2)$$

The values of the thermodynamic functions for PtS_2(c) in the temperature range of 298 – 875 K are calculated using complex integration at the appropriate calculation temperature for PtS_2(к): C_p°(T), S°(T), H°(T) − H°(298.15 K) и Φ°(T)' =−[G°(T) − H°(298.15 K)]/T. Interpolation of the obtained dependences (1) and (2) leaded to the values of $C_p^\circ(PtS_2, cr, 298.15\ K) = 66.23$ J /(mol·K) for the Mayer-Kelly equation (1) and 66.24 J/(mol·K) for the Khodakovsky equation (2). The calculated values are in agreement with the literature data [Westrum] and the value 66.18 ± 0.33 J/(mol·K) which was received by the spline approximation [Iorish] on the basis of authors studies using adiabatic calorimetry in the range from 5- 345 K. The data received in the work can be used for construct ion of the phase diagram S-Pt.

References:

1. Iorish, V.S. and Tolmach, P.I., Procedure and Program for Spline Fitting Low-Temperature Heat Capacity Data // *Zh. Fiz. Khim.*, 1986, vol. 60, №. 10, pp. 2583–2587 (in Russian).
2. Malyshev V.V., Milner G.A., Sorkin E.L., Shibakin V.F. Automatic low-temperature calorimeter // Instruments and Experimental Techniques. 1985. № 6. pp. 195–197 (in Russian).
3. http://www.physics.nist.gov/PhysRefData/Compositions.
4. Khodakovsky I.L. About a new semi-empirical equations of temperature dependence of heat capacity and thermal expansion coefficient of solids Vestnik Otdelenia nauk o Zemle RAN vol. 4, Special Issue, 2012, doi:10.2205/2012NZ_ASEMPG (in Russian).
5. Westrum E.F., Jr., Carlson H.G. Low-Temperature Heat Capacitiesand Thermodynamic Functions of Some Palladium and Platinum Group Chalcogenides. II. Dichalcogenides; PtS_2, $PtTe_2$, and $PdTe_2$. // J. of Chemical Physics. 1961. V. 35. №5. pp. 1670−1676.

Yakovlev O. I., Shornikov S. I. Analysis of experimental data on the olivine evaporation

V. I. Vernadsky Institute of Geochemistry and Analytical Chemistry RAS, Moscow (yakovlev@geokhi.ru)

Abstract. High olivine concentration in chondrites explains the interest of researchers to its primary condensation from a gas phase, and its evaporation at the stage of nebular evolution. The new experimental data on the olivine high-temperature vaporization are appeared in the literature in recent years. All authors both past and modern experimental works suggested that forsterite evaporates congruently (without changing the solid state composition). Evaporation of olivine as a phase of variable composition, occurs in such a way that between the substance in a condensed state (liquid or solid) and in gas phase may be the difference in Fe-contents, while the "olivine" stoichiometry [(Mg + Fe) / Si = 2] remains unchanged. A critical analysis of almost all experimental data showed that actually the process of olivine evaporation from the solid phase (sublimation) is really close to congruent, while the liquid phase evaporation is clearly incongruent. As shown by our study, the olivine evaporation depends on the kinetics of the process. In the evaporation pulsed mode the ratio of the Mg / Si was close to 1, which does not correspond to the olivine stoichiometry and therefore congruent evaporation character.

Keywords: olivine, evaporation.

A high degree of relative content of olivine in chondrites explains the interest of researchers to its primary condensation from a gas phase and its evaporation at the stage of nebular evolution.

In the last decades there were published a lot of experimental works for determining the total pressure of forsterite and the partial pressure of the forsterite components depending on the temperature. Experiments on evaporation were carried out as in the mode of evaporation from the exposed surface in the vacuum and in the quasiequilibrium regime of evaporation in the Knudsen cell with the mass spectrometric determination of the vapor composition. Fig. 1 presents selected foreign and domestic data describing the high temperature evaporation of forsterite. One may notice that they are obtained at relatively low temperatures, seldom exceeding the melting point of the mineral (1890 °C). Thus, Fig. 1 presents mainly data on the vapor pressure of forsterite at its sublimation. Experiments have shown that the main forms of vapor particles above the forsterite were the atomic magnesium (Mg) and molecular suboxide silicon (SiO). The oxygen presented in the vapor in atomic and molecular forms (O and O_2). Fig. 1 shows for comparison the temperature dependence of the vapor pressure of magnesium (MgO) and silicon oxides (SiO_2).

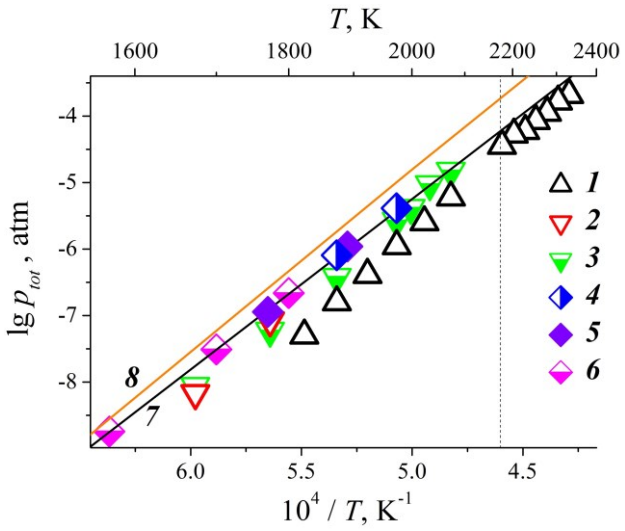

Fig. 1. The total vapor pressure over Mg_2SiO_2 determined: *1* and *2* – to Langmuir (Hashimoto, 1990; Nagahara and Ozawa, 1999), *3–6* – to Knudsen (Nagahara et al., 1994; Kambayashi and Kato, 1983–1984; Stolyarova et al., 2004; Zaitsev et al., 2006), respectively. The total vapor pressure over MgO (*7*) and SiO_2 (*8*) calculated in the present study using the data (Glushko et al., 1978–1982; Shornikov et al., 2000). The dashed vertical line indicates the forsterite melting point.

Many authors both past and contemporary experimental works suggested that forsterite evaporates congruently, i.e. without changing the composition. Moreover, the evaporation of olivine as a phase of variable composition occurs in such a way that between the substance in a condensed state (liquid or solid) and gas may be the difference in FeO contents, but olivine stoichiometry [(Mg + Fe) / Si = 2] remains unchanged, that is, olivine evaporates congruently too.

Critical analysis of experimental data showed, however, that the process of evaporation from the solid phase (sublimation) is really close to congruent, then as evaporation of liquid phase is clearly incongruent in nature. Well known that the sublimation only affects the surface layer of crystalline substances, while leaving the inner part of the crystal unchanged. In this case, the evaporation process can be described as congruent, as the olivine in the process of evaporation keeps generally the unchanging of the composition. However, in the surface layer composition may be essentially different. Interestingly, that at the sublimation of forsterite in a narrow surface zone of a crystal with a thickness of only ~5 microns recorded a strong isotopic fractionation of magnesium (Wang et al., 1999).

As for evaporation from the liquid phase any clear data on the nature of evaporation of olivine melt is absent. Many authors often refer to the results of the work A. Hashimoto (Hashimoto, 1990) where in some experiments the temperature was beyond the melting temperature of forsterite (Fig. 1) and where, as believed, given the proofs of congruence of the melt evaporation. But in reality, there are no any evidences in the Hashimoto's work, while it was written literally the following: "Molten forsterite also evaporates almost stoichiometrically. Only the most highly evaporated residues contained a trace (~5 vol. %) of SiO_2-rich glass (~65 wt. % SiO_2)". Hashimoto's article contains no data on "almost congruent" evaporation of forsterite melt and does not give interpretation on the fact of SiO_2 accumulation in the residual melt.

In recent works on evaporation (Mendybaev et al., 2014) it is also argued that the melts close to forsterite compositions evaporate congruently. However, our calculations of the Mendybaev's and his colleagues analytical data showed the wrongness of this proposition (Fig. 2).

In addition, as shown by our study (Yakovlev et. al., 1995; Gerasimov et. al., 2015) the evaporation of olivine is determined by the kinetics of the process. The results of experiments on of high-mg olivine evaporation in the condition of impact and laser-pulse heating showed that the condensed vapor compositions differed from the residual melt ones. In the conditions of high temperature and rapid evaporation the ratio of elements Mg/Si in a vapor was close to 1 (Fig. 3) that does not correspond to the olivine stoichiometry and, therefore, congruent character of evaporation.

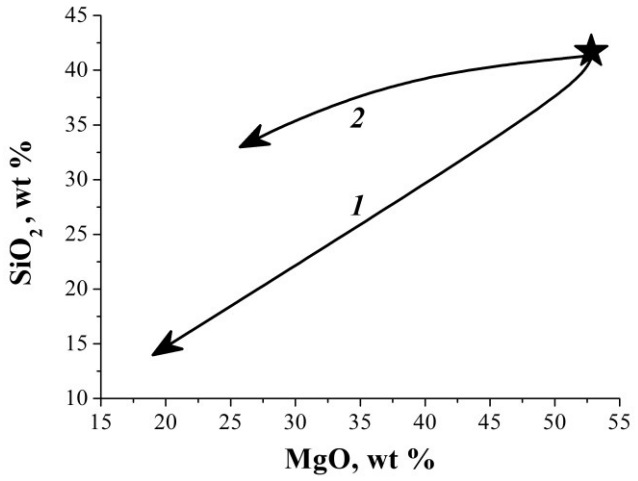

Fig. 2. Estimated and actual evaporation trends of the melt FUN1 evolution according to the Mendybaev's data (Mendybaev et al., 2014). Table of symbols: *1* – evolution trend of the melt FUN1 composition in the case of congruent forsterite evaporation of forsterite; *2* – evolution trend of the melt FUN1 composition in the case of experimental evaporation. Star shows the initial composition of FUN1.

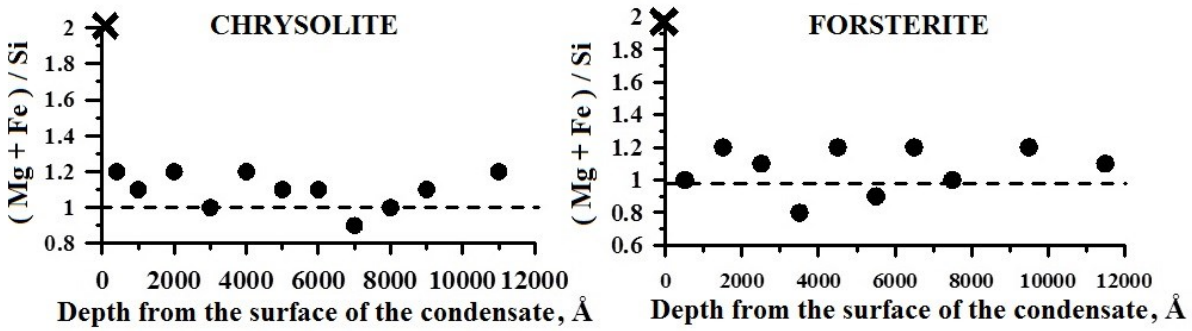

Fig. 3. Ratio variations of (Mg + Fe^{2+}) / Si in the vapor-condensate layers. Cross shows the ratio in the initial olivines.

References:

1. Gerasimov, M. V., M. A. Zaitsev, Yu. P. Dikov, O. I. Yakovlev, K. M. Ryazantsev (2015). Olivine evaporation at pulse high-temperature heating conditions. *Trudy VESEMPG*, vol. 1, pp. 234–237 [in Russian].
2. Glushko, V. P., L. V. Gurvich, G. A. Bergman, I. V. Veitz, V. A. Medvedev, G. A. Khachkuruzov, V. S. Youngman (1978–1982). Thermodynamic properties of individual substances. M.: Nauka.
3. Hashimoto, A. (1990). Evaporation kinetics of forsterite and implications for the early solar nebula. *Nature*, vol. 347, no. 6288, pp. 53–55.
4. Kambayashi, S. and E. Kato (1983). A thermodynamic study of (magnesium oxide + silicon dioxide) by mass spectrometry. *J. Chem. Thermodyn*., vol. 15, no. 6, pp. 701–707.
5. Kambayashi, S. and E. Kato (1984). A thermodynamic study of (magnesium oxide – silicon dioxide) by mass spectrometry at 1973 K. *J. Chem. Thermodyn*., vol. 16, no. 2, pp. 241–248.
6. Mendybaev, R. A., F. M. Richter, C. D. Williams, A. V. Fedkin, M. Wadhwa (2014). Evolution of chemical and isotopic compositions of FUN CAIs: experimental modelling. *LPSC-XLV*, abs. #2782.
7. Nagahara H., I. Kushiro, B. O. Mysen (1994). Evaporation of olivine: low pressure phase relations of the olivine system and its implication for the origin of chondritic components in the solar nebula. *Geochim. Cosmochim. Acta*, vol. 58, no. 8, pp. 1951–1963.
8. Nagahara, H. and K. Ozawa (1999). Mechanism of forsterite evaporation as inferred from surface microstructures. *Proc. Japan Acad. B*, vol. 75, no. 2, pp. 29–34.
9. Shornikov, S. I., I. Yu. Archakov, M. M. Shultz (2000). Mass spectrometric study of evaporation and thermodynamic properties of silica: III. Equilibrium reactions of molecules occurring in the gas phase over silica. *Russ. J. General Chem*., vol. 70, no. 3, pp. 360–370.
10. Stolyarova, V. L., S. I. Lopatin, V. V. Bondar (2004). Thermodynamic properties of the MgO–SiO_2 system by high-temperature mass spectrometry. *Dokl. Phys. Chem*., vol. 399, no. 1, pp. 82–84.
11. Wang, J., A. M. Davis, R. N. Clayton, A. Hashimoto (1999). Evaporation of single crystal forsterite: evaporation kinetics, magnesium isotope fractionation, and implications of mass-dependent isotopic fractionation of a diffusion-controlled reservoir. *Geochim. Cosmochim. Acta*, vol. 63, no. 6, pp. 953–966.
12. Yakovlev, O. I., Yu. P. Dikov, M. V. Gerasimov (1995). Experimental study of shock and pulse evaporation of the ultrabasic substance. *Geochem. Int.*, vol. 33, no. 8, pp. 1235–1247.
13. Zaitsev, A. I., N. A. Arutyunyan, N. G. Shaposhnikov, N. E. Zaitseva, V. T. Burtsev (2006). Experimental study and modeling of the thermodynamic properties of magnesium silicates. *Russ. J. Phys. Chem*., vol. 80, no. 3, pp. 335–344

Ildar V.. Zakirov[1], Valeria A. Suvorova[1], Valentin O. Osadchii[1,2] An experimental study of the solubility of tin in H_2O vapor.

[1]Institute of Experimental Mineralogy RAS, Chernogolovka Moscow district,

[2]M.V. Lomonosov Moscow State University, Department of Geology, Moscow (lera@iem.ac.ru)

Abstract. The solubility of SnO_2 in supercritical water vapor was studied at 400C and 250-290 bar by autoclave method with an in-situ sampling of vapor.

Keywords: tin; water vapor; solubility; cassiterite.

The behavior of tin in hydrothermal geological processes is primarily controlled by the solubility of cassiterite (Migdisov, Williams-Jones, 2005). In the chlorine-free environment, tin is usually present in the form of either $Sn(OH)_2$ or $Sn(OH)_4$ in both aqueous solutions and water vapor. The thermodynamic parameters of the former are well-studied (Cigala, 2012), while the properties of the latter are still unknown. Previously, we reported solubility of SnO2 in water vapor in the system SnO_2-H_2O at 330-360°C and saturated water pressure (Zakirov et al., 2016). In this study, we present solubility of SnO_2 at 400°C and 250-290 bar.

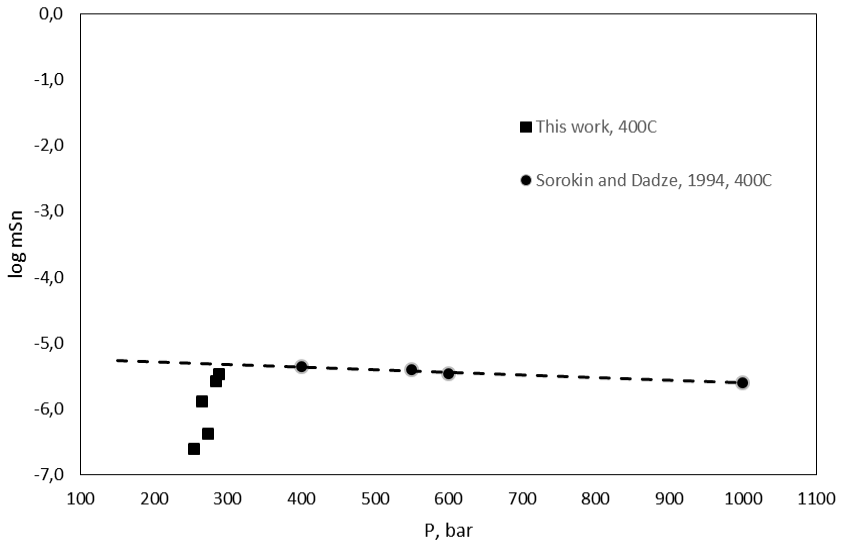

Fig. 1. The solubility of SnO_2 in water vapor

In our experiments, we used distilled deionised water and crystalline tin oxide SnO_2 produced by Sigma-Aldrich.

Experiments were carried out in Ti-based (VT8) autoclave (120 cm^3) with an inner ampoule (13 cm^3) for in situ sampling of the vapor phase. This technique is described in details elsewhere (Zakirov et al., 2007; Akinfiev, Zotov, 2016). The pressure during the runs was measured with a D100 strain gauge calibrated against a standard piston gauge. The autoclave temperature was monitored by the S-type thermocouple. The uncertainties in the pressure and temperature measurements are ±0.3MPa and 2K, respectively. The amount of SnO_2 was at least two orders higher than its solubility in water at the temperature of the experiment.

After heating for 2-3 days (which was enough for the system to equilibrate) the inner capsule was opened for 5 minutes and then closed, the autoclave was removed from the oven and quenched in cold water. After quenching, the capsule containing condensed vapor was rinsed five times with a well-known quantity of aqua regia. These wash solutions were collected, diluted up to 5 times and then analyzed separately by the ICP method.

The measured solubility of cassiterite at 400°C is shown in figure 1. The results are in agreement with a previously measured solubility of cassiterite in supercritical water vapor at 400°C determined by Sorokin and Dadze (1994). This agreement indicates that $Sn(OH)_4$ is the main species of Sn in neutral water solutions.

We are grateful to Ya. V. Bychkova for conducting the ICP-MS analysis and A.V. Zotov for his comments on the experimental part of this study.

References:

1. Akinfiev NN, Zotov A V. (2016) Solubility of chlorargyrite (AgCl(cr./l.)) in water: New experimental data and a predictive model valid for a wide range of temperatures (273–873K) and water densities (0.01–1 $g \cdot cm^{-3}$). Geochim Cosmochim Acta 178:178–194. doi: 10.1016/j.gca.2016.01.027
2. Cigala RM, Crea F, De Stefano C, et al. (2012) The inorganic speciation of tin(II) in aqueous solution. Geochim Cosmochim Acta 87:1–20. doi: 10.1016/j.gca.2012.03.029
3. Migdisov AA, Williams-Jones AE (2005) An experimental study of cassiterite solubility in HCl-bearing water vapour at temperatures up to 350 °C. Implications for tin ore formation. Chem Geol 217:29–40. doi: 10.1016/j.chemgeo.2004.11.018
4. Sorokin VI, Dadze TP (1994) Solubility and complex formation in the systems Hg-H_2O, S-H_2O, SiO_2-H_2O and SnO_2-H_2O. Fluids in the Crust. Springer Netherlands, Dordrecht, pp 57–93
5. Zakirov IV, Suvorova VA, Osadchii VO (2016) An experimental study of solubility of tin in H_2O vapor. Experiment in GeoSciences Vol. 22: P. 51–51.
6. Zakirov IV, Sretenskaja NG, Aranovich LY, Volchenkova VA (2007) Solubility of NaCl in CO_2 at high pressure and temperature: First experimental measurements. Geochim Cosmochim Acta 71:4251–4255. doi: 10.1016/j.gca.2007.01.028

Zharkova E.V., Kadik A.A. Intrinsic oxygen fugacity of zircons of different ages and from different regions - the experimental data.

V.I. Vernadsky Institute of Geochemistry and Analytical Chemistry RAS, Moscow (zharkova@geokhi.ru)

Abstract. We have carried out the electrochemical determination of the intrinsic oxygen fugacity (fO_2) in zircons from continental crustal igneous and metamorphic complexes of various ages, in order to estimate the possible evolution of the redox regime of the lithospheric upper mantle with time. The intrinsic oxygen fugacity values recorded in zircons from the oldest tonalities (orthogneisses) of the Omolon Massif in Siberia with an age of 3500 Ma and granitoids of the granite-greenstone association in the middle Pridnestrovie with an age 3000 Ma indicate that the redox conditions of the Precambrian lithospheric mantle were close to the WM buffer. These fO_2 values are generally consistent with the redox state of "dry" low depleted peridotites. The crystals don't show the oxygen potential as high as the FMQ and FMQ+1 values that are typical of mantle rocks affected by metasomatic alteration. The determination of intrinsic oxygen fugacity in zircons from igneous and metamorphic crystal complexes of various ages shows that these rocks bear evidence of the evolution of redox conditions in the upper mantle, which is related to an increase in oxygen potential after 3000-3500 Ma. However, the fO_2 values of old zircons don't reach the values typical of mineral equilibrium with a metallic iron phase, which characterized the final stages of upper mantle formation. Therefore, significant increase in oxygen potential of the upper mantle occurred at the earlier stages of Earth formation.

Key words: zircon, intrinsic oxygen fugacity, tonalite, orthgneiss, peridotite, redox state, mantle.

Thermodynamic and experimental study of xenoliths reveals a wide variation of oxygen fugacity in the upper mantle, beneath both the continents and oceans [Arculus R.G.; Kadik A.A.]. The determined fO_2 values range between QMF (quartz-magnetite-fayalite) and IW (iron-wustite) buffer equilibria. The evolution of the redox state of the mantle is believed to be generally related to melting, Earth degassing, the formation of the metallic core, and the descent of lithosphere blocks into the mantle. However, our knowledge of the processes that govern the oxygen balance in the Earth's interior is rather limited in many aspects. The evolution of the redox state of the mantle through geologic history is also debatable. It is suggested that the original upper mantle was more reduced than the modern one, its fO_2 values corresponded to mineral equilibria with a (Fe, Ni) metallic phase, and that chemical differentiation of the upper mantle was accompanied by an increase in oxygen potential [Arculus R.G.; Kadik A.A]. However, there is no clear evidence if this process was gradual or occurred at the earlier stages of mantle generation, when the oxygen balance could be affected by degassing or large-scale melting of the mantle at the later stages of Earth accretion.

We have carried out the electrochemical determination of the intrinsic oxygen fugacity in zircon crystals from continental crustal igneous and metamorphic complexes of various ages, in order to estimate the possible evolution of the redox regime of the lithospheric upper mantle with time. Zircon (zirconium orthosilicate) is a very common accessory mineral in various igneous, metamorphic, and sedimentary rocks. It could be a product of primary magmatic crystallization or metamorphic transformation, a xenocryst captured by magma from the wall rocks, or a detritic grain. The high resistance of zircon to chemical or thermal attack, the elevated concentration of uranium substituting for zirconium in the mineral structure, and the lack of affinity to lead enable this mineral to be used for dating rocks by the U-Pb isotope method. The high resistance of zircon to various chemical attacks is well known and is especially favorable for age determinations. The intrinsic oxygen fugacity of oxide minerals has a complex nature and is related to both the existence of elements with variable valence and oxygen defects in mineral structures. Thermodynarnically, fO_2 determined in minerals with a solid-state electrochemical cell indicates the redox conditions during their primary growth [Sato M.], if the natural compounds have not suffered secondary alteration caused by subsequent geochemical processes.

We took 14 samples of zircons of different ages and from different regions in order to determine the intrinsic oxygen fugacity. The description of the sample is in the table 1.

Table 1. The description of samples (the collection E.V. Bibikova) [Bibikova, E.V. et al.]

Sample	Rock	Region	Ages Ma.)
15148	granite	Eastern Zabikalie	130-170
19 a	Rapakivi granite	Berdyaush Pluton. South Ural	1350
8-365	granite	Sharoazarinskii Massif. Eastern Siberia.	340
ONG 3	Plagiogranite	Onot's block. Prisayani'e.	3400
29950	Gabbro	Orekhovo-Pavlograd zone of the Ukrainian Sheild	2650
13-11	Gabbro	Not Lake Intrusive Complex. The Baltic Shield.	2700
2128	Gabbro-	Elenovka. Priazovskii block. The Ukrainian Sheild.	2900

Sample	Rock	Region	Ages Ma.)
	diorite		
C-87-21	Diorite	Kllitch River. The tectonic zone of the Main mountain-ridge of the Big Cavkase.	320
196	Diorite	The region of Tupaiya Guba. Kovd Lake. The Baltic Shield	2730
650	Diorite	Yamburg. Region of the middle Pridnestrov'e area a typical example of the granite-greenstone association.	3000
Chuk10	Orthogneiss	The orthogneisses of the Omolon Massif. Northeastern Siberia is among the oldest rocks of Russia.	3500
3/1	Charnockite	The Aldan's Shield. The sample was taken in the middle flow of the Aldan River.	1970
518	Charnockite	The Vichanskii Massif. The Baltic Shield.	2420
19	kimberlite	Pipe "Mir". Yakutia	350

The measurements of the intrinsic oxygen fugacity were carried out on high temperature furnace based on two solid electrolytes **[**Kadik A.A., Zharkova Ye.V. et al.]. The electrochemical determination of the intrinsic oxygen fugacity of zircons in direct (temperature increase) and reverse (temperature decrease) experiments shows a linear correlation between fO_2 in crystals and inverse temperature (1/T), according to the equation:

$$\log fO_2 = A+B/T^oK, \quad (1)$$

This is indicates that the equilibrium was attained and no side reactions capable of affecting the fO_2 determination occurred in the experiment. The most typical side reactions are related to inclusions in minerals, especially fluid inclusions. Generally, the slope of the log fO_2 versus 1/T curve for zircon (i.e., the value of coefficient "B"*)* is close to that of the oxygen buffer WM (table 2). At temperatures 800-1100°C, the log fO_2 is within ±1 logarithmic unit of the WM oxygen buffer. The "A" and "B" coefficients in the linear equation (1) for zircon are listed in the table 2**.**

Table 2. The values of the coefficients "A" and "B" in the empirical equation 1 for zircons from different rocks and regions and the position of straight line relative to buffer equilibrium QFI, IW, WM and FMQ.

Sample	A	B	r*	n**	The position of straight line relative to buffer equilibrium
15148	23,046	45430	0,993	10	At 800ºC ±1 log unit fO_2 IW. At 1100ºC ±1,5 log unit fO_2 FMQ
19 a	20,814	42121	0,996	9	
8-365	16,407	37805	0,991	9	
ONG 3	32,494	55912	0,998	8	
29950	26,183	48686	0,974	9	800ºC –IW; 1100ºC FWQ
13-11	9,358	30775	0,985	8	Practically coincide with buffer IW
2128	9,546	31274	0,977	9	
C-87-21	12,335	34333	0,975	8	Between buffers IW и WM
196	17,312	38581	0,981	8	
650	12,843	32531	0,989	9	
Chuk 10	14,509	35680	0,988	9	Between buffers IW and WM
3/1	14,702	35501	0,991	8	WM ±1 log unit fO_2
518	18,794	39012	0,967	13	
19	10,994	32230	0,978	8	Near to IW

Note: n*- the quantity of experimental points, r** coefficient of correlation.

The zircons studied electrochemically bear evidence of the magmatic origin and complex petrological history of their host rocks. The measured oxygen fugacity in these crystals reflects probably the whole complex of processes that occurred in the lithosphere in geologic history. Subsequently, the interpretation of events that controlled the fO_2 values of zircons is rather difficult.

Let us compare the fO_2 values obtained for zircons of crustal igneous and metamorphic complexes of various ages with fO_2 values recorded in the rocks of the upper mantle. The reactions involving Fe^{2+}-Fe^{3+} equilibrium in the polymineral systems of the upper mantle rocks show that the redox state of the modern continental and oceanic lithospheric mantle is highly variable [Arculus R.J.; Ballhaus C.; Kadik A.A., Zharkova Ye.V. et al.] The highest fO_2 values exceed that of the QMF buffer, whereas the lowest estimates are 2-3 orders of magnitude lower than the QMF buffer [Arculus R.J.; Ballhaus C.; Kadik A.A., Zharkova Ye.V. et al.]. However, average fO_2 values are close to the QMF buffer. The measured fO_2 values for asthenospheric rocks are normally 2-3 orders of magnitude lower than the QMF buffer [Arculus R.J.; Ballhaus C.; Kadik A.A., Zharkova Ye.V. et al.]. The peridotites with high fO_2 bear evidence of metasomatic transformation and are extremely depleted [Ballhaus C.]. These data indicate that the evolution of the redox state was related to effects of melting and fluids on these rocks.

The values of the intrinsic oxygen fugacity recorded in zircons from the oldest tonalites (orthogneisses) of the Omolon Massif in Siberia with an age of 3500 Ma and granitoids of the granite-greenstone association in the middle Pridneprov'e with an age of 3000 Ma indicate that the redox conditions of the Precambrian lithospheric mantle were close to the WM buffer. These fO_2 values are generally consistent with the redox state of a "dry" low-depleted peridotite. The crystals do not show the oxygen potential as high as the QMF and QMF + 1 values that are typical of mantle rocks affected by metasomatic alteration.

Determination of intrinsic oxygen fugacity in zircons from igneous and metamorphic crustal complexes of various ages shows that these rocks bear evidence of the evolution of redox conditions in the upper mantle, which is related to an increase in oxygen potential after 3000-3500 Ma. However, the fO_2 values of old zircons do not reach the values typical of mineral equilibrium with a metallic iron phase, which characterized the final stages of upper mantle formation. Therefore, significant increase in the oxygen potential of the upper mantle occurred at the earlier stages of Earth formation.

This study was supported by the Russian Foundation for Basic Research No 17-05-20110g

References:

1. Arculus, R.J. Oxidation Status of the Mantle: Past and Present. 1985 Annu. Rev. Earth Planet. Sci. V. 13. P. 75-95.
2. Ballhaus, C. Redox States of Lithospheric and Asthenospheric Upper Mantle.1993. Contrib. Mineral. Petrol. V. 114. P. 331-348.
3. Bibikova, E.V., Ustinov, V.I. et al. 1982. Investigation of Variations of Oxygen Isotope Composition in Accessory Zircon, Dokl. Akad. Nauk SSSR. V. 264, No. 3. P. 698-702.
4. Kadik, A.A. 1997. Evolution of Earth's Redox State During Upwelling of Carbon-Bearing Mantle, Phys. Earth Planet. Inter. V. 100, P. 157-166.
5. Kadik A.A., Zharkova E.V. et al. 1989. Upper Mantle Redox Conditions: Oxygen Fugacity Measurement on Peridotite Xenoliths from the Shavaryn Tsaram Volcano, Mongolia. Geochemistry International. V. 26. No 1. P.12-19.
6. Sato M. 1971. Electrochemical Measurements and Control of Oxygen Fugacity and the Other Gaseous Fugacities with Solid Electrolyte Systems. Research Techniques for High Pressure and High Temperature. Ulmer G.C., Ed., Berlin: Springer. P. 43-99.